SAND2000-3209J

Highly Unstable Double-Diffusive Finger Convection in a Hele-Shaw Cell: Baseline Experimental Data for Evaluation of Numerical Models

Scott E. Pringle[1], Clay A. Cooper[2], and Robert J. Glass[1]

[1]Flow Visualization and Processes Laboratory, Sandia National Laboratories, Alb., NM. U.S.A
[2]Division of Hydrologic Sciences, Desert Research Institute, Reno, NV. U.S.A

ABSTRACT

An experimental investigation was conducted to study double-diffusive finger convection in a Hele-Shaw cell by layering a sucrose solution over a more-dense sodium chloride (NaCl) solution. The solutal Rayleigh numbers were on the order of 60,000, based upon the height of the cell (25 cm), and the buoyancy ratio was 1.2. A full-field light transmission technique was used to measure a dye tracer dissolved in the NaCl solution. We analyze the concentration fields to yield the temporal evolution of length scales associated with the vertical and horizontal finger structure as well as the mass flux. These measures show a rapid progression through two early stages to a "mature" stage and finally a "rundown" period where mass flux decays rapidly. The data are useful for the development and evaluation of numerical simulators designed to model diffusion and convection of multiple components in porous media. The results are useful for correct formulation at both the process scale (the scale of the experiment) and effective scale (where the lab-scale processes are averaged-up to produce averaged parameters). A fundamental understanding of the fine-scale dynamics of double-diffusive finger convection is necessary in order to successfully parameterize large-scale systems.

Key words. double-diffusive convection, instability, porous media

DISCLAIMER

DISCLAIMER

Portions of this document may be illegible in electronic image products. Images are produced from the best available original document.

1. INTRODUCTION

When multiple density-affecting solutes are layered in a buoyantly stable configuration (light over dense), the dissimilar molecular diffusion coefficients can lead to small-scale, hydrodynamic instabilities. This process, referred to as double-diffusive convection, develops features that are much different than those associated with stable advective, dispersive, and/or diffusive transport, and can significantly influence mass transfer when it occurs (Turner, 1979).

Numerical simulations of double-diffusive convection can contribute valuable insight into system behavior (Shen and Veronis, 1991, 1997; Chen and Chen, 1993; Shen, 1995; Stockman et al., 1998). In order to properly constrain such investigations, laboratory experiments are required. The availability of experimental data sets for this purpose, however, is limited due to the difficulties in obtaining high resolution, full-field, non-intrusive measurements. Lambert and Demenkow (1971) and Kazmierczak and Poulikakos (1987) applied non-intrusive methods using polarimetry and laser absortiometry, respectively, to obtain solute concentration and profile measurements. More recently, Cooper et al. (1997; 2000 in review) applied a non-intrusive light transmission technique to the study of double-diffusive systems in a Hele-Shaw cell that allows for full-field, high spatial and temporal resolution. However, these experiments were begun by pulling a divider separating two solutions, resulting in an ambiguous initial condition that makes comparison to simulation problematic.

In this work, we present a data set for highly unstable, double-diffusive finger convection characterized by rapidly developing, nonlinear behavior. An experiment was conducted in a Hele-Shaw cell (an analog of porous media) with sucrose overlying sodium chloride (NaCl). We refined the experimental system of Cooper et al. (1997) to yield a well defined, near step-function initial condition and used light transmission methods to track the evolution of the concentration field in time. As an example of several integral measures that can be obtained from the data, we also present the time evolution of horizontally averaged vertical profiles, the height of the finger region, mass transfer, mass flux, and a characteristic horizontal length scale. These data, both the

concentration fields and integral measures, provide very extensive and high quality data suitable for the development and evaluation of numerical simulators.

2. EXPERIMENTAL DESIGN

Our experiment was conducted in a Hele-Shaw cell with NaCl and sucrose as the diffusing components. The dimensionless buoyancy ratio ($R_\rho = \beta_1 C_1 / \beta_2 C_2$), where β is the volumetric expansion coefficient [dimensionless], and C is the initial solute concentration [dimensionless], was chosen at 1.2 and the solute concentrations were defined to give component (i) Rayleigh number $\left(Rs_i = \beta_i C_i g h k / D_i \upsilon_i\right)$ magnitudes < 60,000. The subscripts 1 and 2 refer to the NaCl and sucrose solutions, respectively, g is acceleration of gravity in the plane of the cell [L t^{-2}], h is the system length scale [L] (here defined as the height of the cell), k is the intrinsic permeability [L^2], D is the molecular diffusion coefficient [L^2 t^{-1}], and υ is the kinematic viscosity [L^2 t^{-1}]. Table 1 presents the fluid properties used in this study. A dye tracer (Warner Jenkins FD&C Blue #1, 0.25 gm/kg) was mixed with the NaCl solution to visualize and quantify the evolving structure. We actually measure the dye concentration, but because the dye has a negligible effect on solution density and the system is highly convective, the tracer is assumed to track the NaCl solution throughout most of the experiment.

The Hele-Shaw cell consisted of two polished glass plates (30.5×19×1.27 cm) separated by plastic shims along their long axis edges, clamped together within an aluminum frame (see Figure 1). The cell was placed onto a test stand (angle at 25° from horizontal) that consisted of a controlled output light source (a two-dimensional array of fluorescent bulbs) and CCD camera (Photometrics, with Kodak KAF-4200 Scientific Grade chip having an array of 2033 × 2048 pixels, each with 4096 gray levels). Images of the entire cell including a constant optical density step wedge were acquired with a spatial resolution of 0.0154 cm. Details of the image acquisition system are discussed in

Detwiler et al. (1999). The temperature of the glass plates was monitored during the experiment at a number of points (average of 21.7°C in time and space with a range of 21.3 to 21.9°C).

The development of the initial condition is shown in Figure 2. The cell was first saturated with water and then the experimental solutions entered from points in the upper and lower corners of the Hele-Shaw cell and exited at a point sink at the opposite side. After ~ 200 cell volumes of fluid was flushed through the cell, the inflow and outflow valves were closed and the instability was allowed to evolve naturally. Analysis of the initial condition using single pixel-wide vertical transects across the cell shows a mean transition zone thickness of 1.2 mm with a variance of 1.3×10^{-5} mm^2. The relative flatness of the interface and its variation in thickness across the cell are shown in Figures 3 and 4, respectively. Figure 3 shows that the interface fluctuates no more than 1.5 mm from the center of the cell. Figure 4 illustrates that the thickness of the interface is relatively constant with a maximum deviation near the inflow boundary.

2.1. Porous Media Analogy

The Hele-Shaw cell provides a clear, unobstructed view of the double-diffusive fingers as they develop that is difficult to achieve in real or artificial porous media. Low Reynolds number [$O(1)$] flows between parallel plates can approximate behavior of two-dimensional flows through porous media (Bear, 1988). For the analogy to be valid, certain criteria must be satisfied that relate the aperture gap to the flow dynamics (Wooding, 1960; Elder, 1967):

$$\frac{\langle a \rangle}{\delta} << 1 \qquad \frac{U\langle a \rangle^2}{\delta \upsilon_c} << 1 \qquad \frac{U\langle a \rangle^2}{\delta D_c} << 1 \qquad \text{(1 a-c)}$$

where $\langle a \rangle$ is the mean spacing between the glass plates, δ is the smallest length scale of motion (i.e, finger width), U is a characteristic velocity, υ_c and D_c are a characteristic kinematic viscosity

and diffusion coefficient of the fluid. The first criterion suggests that the analogy does not hold until the smallest length scale of motion becomes much greater than the cell gap. The second and third criteria imply that inertial effects must be negligible in comparison to the diffusion of momentum and mass. Inequalities 1a and b were satisfied within several minutes of the start of the experiment; that is, by the time the initial perturbations were first observed. However, the third criterion is never fully satisfied. For an individual finger, the value of the left-hand side (essentially a Peclét number) ranges from 3.5 at the start of the experiment to 0.33 when the finger region has reached the boundaries. This implies that there may be a significant component of mass transfer in the third dimension (across the cell gap) so that the concentration fields are not strictly two-dimensional. This may be important in modeling as we discuss in our concluding remarks.

2.2. Aperture and Concentration Fields

The mean aperture was calculated based on the injection of a known mass of liquid into the dry Hele-Shaw cell. The area occupied by the liquid was obtained using an adaptive thresholding algorithm (Nicholl and Glass, 1994), and knowledge of the liquid density resulted in a mean aperture, $\langle a \rangle$, of 0.177 mm $\pm$0.001 mm. The intrinsic permeability (k) was calculated using the relationship $\langle a \rangle^2 / 12$ yielding a value of 2.61×10^{-9} m^2 $\pm$ 10^{-12} m^2.

Application of the protocol of Detwiler et al., (1999) allowed measurement of the aperture field with a root mean square (RMS) error estimated at 0.8% of the mean aperture. The aperture field has a narrow distribution with a variance about the mean of 2.5×10^{-7} cm^2. The x and z-direction semivariograms of the aperture field are presented in Figure 5. The slight trend in the x-direction is due to the fabrication of the glass and the fact that although the plates were polished to a specific tolerance, they are not perfectly flat. The larger trend in the z-direction is a consequence of the clamping pressures along the long sides of the cell. Characterization of the dominate trend (z-direction) in Figure 6 shows the percent variation from the mean aperture based on a horizontally

averaged vertical profile of the aperture field. Table 2 provides a summary of the geometry and statistics of the aperture field.

Following the procedure described by Detwiler et al. (2000), pixel based calibration curves relating light absorbance to dye concentration were built by filling the cell with a series of dye concentrations in a base NaCl solution equal to that used in the experiment. One hundred images were acquired at each concentration, intensity adjusted for slight temporal fluctuations in the light source using the constant optical density step wedge and averaged to effectively remove CCD noise. The resulting pixel-by-pixel calibration curve was characterized by correlation coefficients above 0.99. From single images acquired during the experiment, we obtained concentration fields with maximum precision based average RMS concentration errors of ~ 3% of the maximum solution concentration. Since measures for length scales and mass transfer rates are based on the average of thousands to millions of concentration field data points, this precision-based error becomes negligible in these measures. Evaluation of the mass balance in time suggested that the sucrose concentration also slightly influences the absorbance versus concentration relationship. To compensate for this influence, we applied a small concentration-dependent correction factor (a sine function) to the measured calibration curve. This approach substantially decreased mass balance error from a maximum of 4% to 0.5% at the end of the experiment.

3. CONCENTRATION FIELDS AND STRUCTURAL MEASURES

The experiment lasted 945 minutes with a total of 270 images acquired sequentially in blocks of 45 each with increasing separations in time (0.33, 0.67, 1.33, 2.67, 5.34 and 10.67 minutes). Below, we first present the temporal history as illustrated in a series of normalized concentration field (C/C_o) images. Next, we consider several integral measures that can be obtained from these

concentration fields such as vertical concentration profiles, height of the finger region, mass transfer, mass flux, and a characteristic horizontal length scale.

3.1. Description of Evolving Instability

Figure 7 (a-l) shows a sequence of images spanning the duration of the experiment. The instability develops as a horizontal array of vertical perturbations across the cell. The first detectable perturbations occur at 2.7 minutes into the experiment (based on power spectrum analysis with 95% confidence). These perturbations quickly self-organize into an array of fingers that rapidly grow in time. After approximately 6 minutes, a transition occurs where vertical growth slows as fingers begin to interact and merge with neighbors causing a re-organization of the initial finger structure. Figure 7a shows the convecting field after 11 minutes near the end of this re-organization period.

After re-organization, newly generated fingers continuously form within the transition zone and quickly merge with, and convect up, the stems of nearby, more mature, fingers, eventually reaching the mature finger tip. This process allows a set of fingers that have developed from onset to grow throughout the experiment (Figure 7b,c). In general, the finger appearance consists of a thick 'root' region (located in the transition zone and from where new fingers develop), a somewhat thinner 'stem,' with a transition to a slightly bulbous-like finger tip. The upward and downward moving fingers appear to grow symmetrically about the transition zone. Another interesting feature is the complex, random bifurcation of finger tips (Figure 7d at 96 minutes, see top middle; bottom left and right region).

After 126 minutes (Figure 7e), the fastest growing fingers reach the top and bottom of the cell and begin to spread laterally forming more dense (at the bottom) and less dense (at the top) 'clouds' of fluid. Figures 7f, g, and h show the clouds extending toward the center of the cell. After 216

minutes of convection, isolated pockets of pristine solution ($C/C_o = 1$ or 0) located near the middle of the cell (Figure 7h) continue to generate new fingers until they are eventually exhausted (Figure 7k). At late time (945 minutes) the normalized concentration field throughout the cell approaches homogeneity with the mean C/C_o ranging between 0.4 to 0.6 (Figure 7l). At this point, the system has become dominated by diffusion; structures seen in Figure 7k simply become more diffuse in Figure 7l.

3.2. Integral Measures in Time

The C/C_o fields measured throughout the experiment can be interrogated in a number of ways to yield integral measures of the evolving concentration fields. Horizontally averaged vertical profiles can be developed in time over the course of the experiment (Figure 8). By defining the upper and lower bounds on the profiles, the vertical growth of the finger region (the distance that encompasses the convecting layer) can be determined. In Figure 9 the height of the finger region in time is presented for C/C_o limits of 0.95 and 0.05. There are four different regions of behavior shown in Figure 9: (1) a stable stage (prior to onset of instability), (2) an early stage which includes the initial vertical growth and the transition period when the initial fingers re-organize, (3) a mature stage where the finger region continuously increases, and (4) a rundown stage. The time for the finger region to reach the boundaries is also shown. The growth rate of the finger region during the mature stage results in a velocity of 0.0022 cm s^{-1}. The constant data in Figure 9 within the rundown stage implies that the fingers have convected the entire vertical height of the cell.

A simple Newton-Cotes integration scheme was applied to the C/C_o profile data to obtain the normalized dye/NaCl mass transfer (M/M_o) across the centerline of the cell in time (Figure 10), where M_o is the total mass of dye/NaCl in the cell. Approximately 50% of the available solute mass was transferred from the bottom half of the cell to the top within 300 minutes. The corresponding

normalized mass flux was obtained by dividing the mass transfer by the cross sectional area of the cell and applying a five-point central difference scheme in time (Figure 11, crosses). The 'noise' in the normalized mass flux is far above that due to error in the C/C_o fields and is the result of complexity inherent in the unstable process. A smoothed normalized mass flux is also presented where a moving average of 10 points was applied (Figure 11, circles). The normalized mass flux ($L^{-2}\,t^{-1}$), obtained from the mature stage data, is near constant at a value of 0.64 $m^2\,s^{-1}$. The early stage behavior in the flux that is evident in Figure 10 was also observed in the numerical simulations of Shen and Veronis (1991).

As can be seen in Figure 7, a horizontal length scale that characterizes the evolving concentration field is a function of not only time, but also of the vertical location within the cell. Here we consider a horizontal length scale defined by dividing the cell length by the number of C/C_o slope changes in a horizontal traverse at the centerline of the cell (Figure 12). Considering only the mature stage, we find power law behavior with $\sim t^{0.54}$.

4. CONCLUDING REMARKS

Double-diffusive finger convection occurs when a fluid containing two solutes becomes unstable to perturbations. We conducted an experiment to investigate the evolution of double-diffusive finger convection in a Hele-Shaw cell under a highly unstable initial condition. A lighter sucrose solution was layered over a denser sodium chloride solution containing a dye in a well-defined, near step function initial configuration. Perturbations at the interface quickly form and evolve into mm- to cm-scale fingers that travel primarily vertically, transporting mass at a rate much faster than would occur in a stable diffusive system. As the system evolves, a transition occurs where adjacent fingers begin to merge to form wider fingers, and new fingers begin to be generated from near the

initial concentration step. Over time, this convection-dominated system runs down and becomes dominated by diffusion.

We used a Hele-Shaw cell as an analog to a two-dimensional porous medium. It allows one to resolve with extreme detail the concentration field of a solute and measure the structural patterns that form. However, Hele-Shaw cells are not perfect analogs, and in our highly unstable experiment, one of the conditions for analogy was violated such that concentration fields were not fully two-dimensional. In preliminary simulations using a lattice-Boltzmann approach, recognition of the three-dimensional nature of the field has been shown to be important (Stockman et al., 1998). We also note that natural porous media is not two-dimensional, homogeneous, and isotropic as are Hele-Shaw cell models. Additionally, for scales of motion on the order of the size of a pore, a Hele-Shaw cell may not capture exactly the analogous behavior that would occur in porous media.

In order to quantify the observed behavior, we introduced a dye that is assumed to behave passively; that is, it is assumed to travel in the convective flow field and not undergo motion of its own. This is justified by determining the Peclét number (*Pe*) of dye traveling in a finger. For the values reported above (v~10^{-3} cm sec^{-1}, D (dye)~10^{-10} m^2 sec^{-1}) and a 10 cm long finger, Pe~10^3. Thus, barring chemical reactions and surface phenomena, the diffusion of dye probably has negligible effect on our results while convection is dominant. However, the dye will not fully map NaCl, especially at longer times when diffusion begins to dominate. Simulations of the experiments should be considered that include a passive tracer as actually measured in the experiment.

The data presented in this paper provides a baseline for use in the development and evaluation of models for double-diffusive systems. There are two types of models that must be developed. The first, which we call 'process level,' is formulated at the scale of the experiment in order to simulate

the full complexity of the evolving flow field. Once evaluated, process level models can be extended to consider more than two density-affecting components as well as precipitation/reaction mechanisms that will also influence local fluid composition and density. The second type of model, which we call 'effective level,' is formulated at larger scales and must capture the essence of the enhanced flux in an effective large-scale sense. While necessary for regional-scale hydrogeological analyses where it is impossible to resolve the fine-scale structures as seen here, such an approach will be a challenge to develop and will require additional fundamental understanding of the double-diffusive process so that appropriate process up-scaling can be formulated.

ACKNOWLEDGMENTS

Experimental data was obtained with financial support from the U.S. Department of Energy's Basic Energy Sciences Geoscience Research Program under contract numbers DE-AC04-94AL85000 (Sandia National Laboratories) and DE-FG03-96ER14611 (Desert Research Institute). Analysis and presentation of the data in this paper were accomplished with funds from the Geoscience Center at Sandia National Laboratories and the Division of Hydrologic Sciences at the Desert Research Institute. We thank Anthony Chavez for his work in constructing the test stand and Mark Haagenstad for his assistance with construction of the Hele-Shaw cell. All data presented in this paper are available and can be obtained by contacting the first author.

REFERENCES

Bear, J., 1988, *Dynamics of Fluids in Porous Media*, 764 pp., Dover, New York.

Chen, F. and Chen, C. F., 1993, Double-diffusive fingering convection in a porous medium, *Int. J. Heat Mass Transfer*, **36**, 793-807.

Cooper, C. A., Glass, R. J., and Tyler, S. W., 1997, Experimental investigation of the stability boundary for double-diffusive finger convection in a Hele-Shaw cell, *Water Resour. Res.*, **33**(4), 517-526.

Cooper, C. A., Glass, R. J., and Tyler, S. W., 2000, Double-diffusive finger convection: Flow field evolution in a Hele-Shaw cell, in review at *Water Resour. Res.*

Detwiler, R. L., Pringle, S. E., and Glass, R. J., 1999, Measurement of fracture aperture fields using transmitted light: An evaluation of measurement errors and their influence on simulations of flow and transport through a single fracture, *Water Resour. Res.*, **35**, 2605-2617.

Detwiler, R. L., Rajaram, H., and Glass, R. J., 2000, Solute transport in variable-aperture fractures: An investigation of the relative importance of Taylor dispersion and macrodispersion, *Water Resour. Res.*, **36**(7), 1611-1625.

Elder, J. W., 1967, Steady free convection in a porous medium heated from below, *J. Fluid Mech.*, **27**, 29-48

Irani, R. R., and Adamson, W., 1958, Transport processes in binary liquid systems. I. Diffusion in the sucrose-water system at 25°. *J. Phys. Chem.* **62**, 1517-1521.

Kazmierczak, M. and Poulikakos, P., 1987, On optical technique for the in-situ measurement of species concentration in double diffusive convection. *Int. Comm. Heat Mass Transfer,* **14**, 3-10.

Lambert, R. B. and Demenkow, J. W., 1971, On the vertical transport due to fingers in double diffusive convection, *J. Fluid Mech.*, **54**, 627-640.

Nicholl M. J. and Glass, R. J., 1994, Wetting phase permeability in a partially saturated horizontal fracture, paper presented at the 5th International Conference of High Level Radioactive Waste Management, Am. Nucl. Soc., Las Vegas, Nev.

Shen, C. Y., 1995, Equilibrium salt-fingering convection, *Phys. Fluids*, **7**, 707-717.

Shen, C. Y. and Veronis, G., 1991, Scale transition of double-diffusive finger cells, *Phys. Fluids A*, **3**, 58-68.

Shen, C. Y., and Veronis, G., 1997, Numerical simulation of two-dimensional salt fingers, *J. Geophys. Res.*, **102**, 23131-23143.

Stockman, H. W., Glass, R. J., Cooper, C., and Rajaram, H., 1998, Accuracy and computational efficiency in 3D dispersion via lattice-Boltzmann: Models for dispersion in rough fractures and double-diffusive convection, *Int. J. Modern Phys. C*, **9**, 1545-1557.

Stokes, R. H., 1950, The diffusion coefficients of eight univalent electrolytes in aqueous solution at 25°. *J. Am. Chem. Soc.*, **72**, 2243-2247.

Turner, J. S., 1979, *Buoyancy Effects in Fluids*, Cambridge, 368 pp.

Weast, R. C. (Ed.), 1977, *CRC Handbook of Chemistry and Physics*, 57th ed., CRC Press, Boca Raton, Fla.

Wooding, R. A., 1960, Instability of a viscous liquid of variable density in a vertical Hele-Shaw cell, *J. Fluid Mech.*, **7**, 501-515.

FIGURE CAPTIONS

Figure 1: Schematic of the experimental set up. Hele-Shaw cell aperture is initially saturated with water. Sodium chloride (NaCl) and sucrose solutions enter the cell from the top and bottom corners and exit at a point sink at the opposite side. Fluid properties are such that the molecular diffusivity and density of NaCl solution (D_1, ρ_1) are greater than the sucrose solution (D_2, ρ_2).

Figure 2: Temporal development of the initial transition zone between the NaCl-sucrose solution. Dimensions of the flow field are 25.41 × 16.25 cm. (a) shows the dyed NaCl solution entering from the left corner of the cell at 0.5 minutes (sucrose, entering at the top left corner, mirrors the development of the NaCl solution but can not be seen because no dye was placed in the sucrose solution). (b) at 1 minute, the solutions converge in the center of the cell and a distinct transition zone between the two solutions form. (c) after 30 minutes (~ 200 cell volumes) the inflow and outflow valves are closed and the static transition zone is well defined (thickness ~ 0.12 cm) with less-dense sucrose solution (black) above more-dense NaCl solution (red).

Figure 3: The variation about the center of the transition zone ($C/C_o = 0.5$) with horizontal distance from left boundary. A variation of ~ 0.1 cm occurs near the left and center of the cell with deviations at right boundary of ~ 0.15 cm.

Figure 4: The variation about the mean transition zone at the beginning of the experiment (time = 0) as a function of horizontal distance from left boundary. In general, the deviation from the mean (1.2 mm) is within 5%. At the left boundary there is a maximum variation of 12%, and this is due to the transition between dynamic flow (setting up the transition zone) and static initial conditions (when the inflow and outflow valves are closed). The small variations in the transition region thickness along the horizontal length allow for natural, unperturbed evolution of the fingers.

Figure 5: Semivariogram (normalized to aperture variance) of the x (horizontal) and z (vertical) directions of the aperture field represented by the dashed and solid lines, respectfully.

Figure 6: Variation from the mean aperture as function of distance from top boundary. The clamping pressures along the top and bottom boundaries of the glass plates required for cell construction causes 'bowing' which results in a larger aperture (2.5% of mean) at the center and smaller aperture (- 3.5% of mean) at the boundaries.

Figure 7(a-d): Normalized concentration fields (C/C_o) of the evolving double-diffusive convection based on percent of NaCl mass transferred in the vertical direction. (a) 1% mass transfer at t = 11 minutes, (b) 5% mass transfer at t = 39 minutes, (c) 10% mass transfer at t = 68 minutes, (d) 15% mass transfer at t = 96 minutes. C/C_o in legend refers to normalized concentration of NaCl solution.

Figure 7(e-h): Continued from Figure 7(a-d). (e) 20% mass transfer at t = 126 minutes, (f) 25% mass transfer at t = 156 minutes, (g) 30% mass transfer at t = 180 minutes, (h) 35% mass transport at t = 216 minutes. C/C_o in legend refers to normalized concentration of NaCl solution.

Figure 7(i-l): Continued from Figure 7(e-h). (i) 40% mass transfer at t = 232 minutes, (j) 45% mass transfer at t = 306 minutes, (k) 50% mass transfer at t = 528 minutes, (l) 51% mass transfer at t = 945 minutes. C/C_o in legend refers to normalized concentration of NaCl solution.

Figure 8: Horizontally averaged vertical profiles of the normalized concentration (C/C_o) field at selected times during the experiment (time history indicated by arrow).

Figure 9: The growth of finger region based on normalized concentration profile limits that characterize the maximum growth of the fingers in time (C/C_o = 0.95 and 0.05). There are four

stages that occur during the experiment. These are the stable stage (before the onset of instability), the early stage which includes the initial vertical growth followed by a leveling off period, the mature stage where vertical growth continues, and the rundown stage where the interactions of the fingers with the boundaries begins to influence finger behavior. The time at which the finger region contacts the upper and lower boundaries is indicated by the arrow.

Figure 10: Normalized mass transfer (M/M_o) as a function of time. See Figure 9 caption for description of stages.

Figure 11: Normalized mass flux as a function of time. See Figure 9 caption for description of stages. A five-point central difference algorithm was applied to M/M_o data (crosses) and moving average (of 10) was applied to smooth data (circles).

Figure 12: Horizontal finger width as a function of time. See Figure 9 caption for description of stages. Finger widths are defined for the transition zone region based on a computer code that detects concentration gradients between adjacent fingers. Due to the slight curvature of the transition zone at early time, it takes ~ 5 minutes for all fingers to convect far enough to be detected by the code; therefore, these data (diagonal crosses) are inferred. For time > 60 minutes code gives erroneous results due to difficulty in detecting the decreasing gradients.

Table 1: Fluid properties

Property	Value	Stdev
C_1 (g/kg)	34.6328	6×10^{-4}
C_2 (g/kg)	52.3415	1×10^{-3}
β_1	0.689	3×10^{-3}
β_2	0.372	2×10^{-3}
D_1 ($m^2 s^{-1}$)	1.48×10^{-9}	2×10^{-11}
D_2 ($m^2 s^{-1}$)	4.88×10^{-10}	9×10^{-12}
D_3 ($m^2 s^{-1}$)	5.67×10^{-10}	1×10^{-11}
υ_2 ($m^2 s^{-1}$)	1.03×10^{-6}	2×10^{-8}
υ_1 ($m^2 s^{-1}$)	1.13×10^{-6}	2×10^{-8}
Rs_1	-27,625	800
Rs_2	62,700	1800

Subscript 1 and 2 refer to NaCl and sucrose solution respectively

Properties reported are based on initial conditions (time = 0)

β (volumetric expansion cofficient) from density versus concentration data (Weast 1977)

D_1 (NaCl diffusion coefficient) from Stokes (1949) and D_2 (sucrose diffusion coefficient) from Irani and Adamson (1958) at 50% of the maximum concentration which represents the average concentration of each solution within the transition zone

D_3 (dye diffusion coefficient) from Detwiler et al. (2000)

υ (kinematic viscosity) from Weast (1977)

Table 2: Aperture field dimensions and measured statistics

Dimensions, cm x cm	25.41 x 16.25
Pixel size, cm	1.54×10^{-2}
<a>, cm	1.77×10^{-2}
Minimum aperture, cm	1.70×10^{-2}
Maximum aperture, cm	1.81×10^{-2}
RMS Error, % of mean	0.8

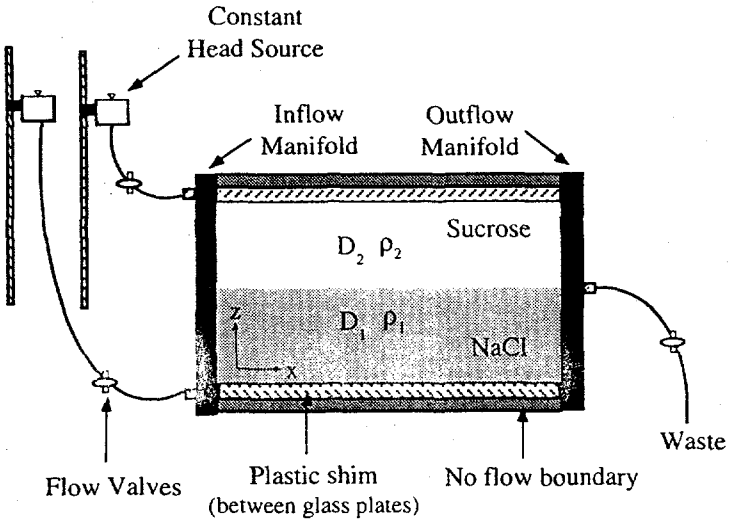
Constant
Head Source
Inflow
Manifold
Outflow
Manifold
Sucrose
D_2 ρ_2
z
x
D_1 ρ_1
NaCl
Waste
Flow Valves
Plastic shim
(between glass plates)
No flow boundary

F1


0
C/Co
1

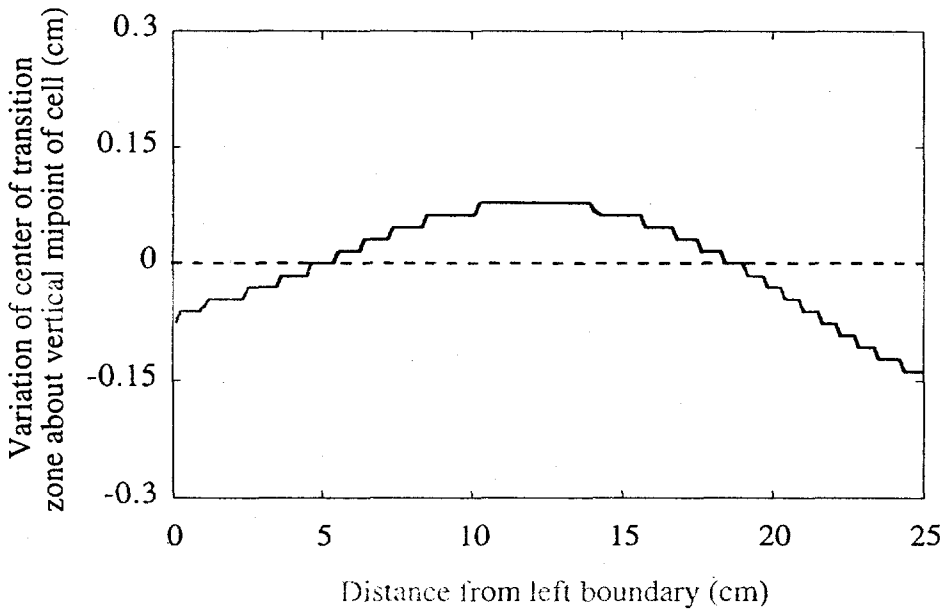
Variation of center of transition zone about vertical mipoint of cell (cm)
0.3
0.15
0
-0.15
-0.3
0
5
10
15
20
25
Distance from left boundary (cm)

F 3

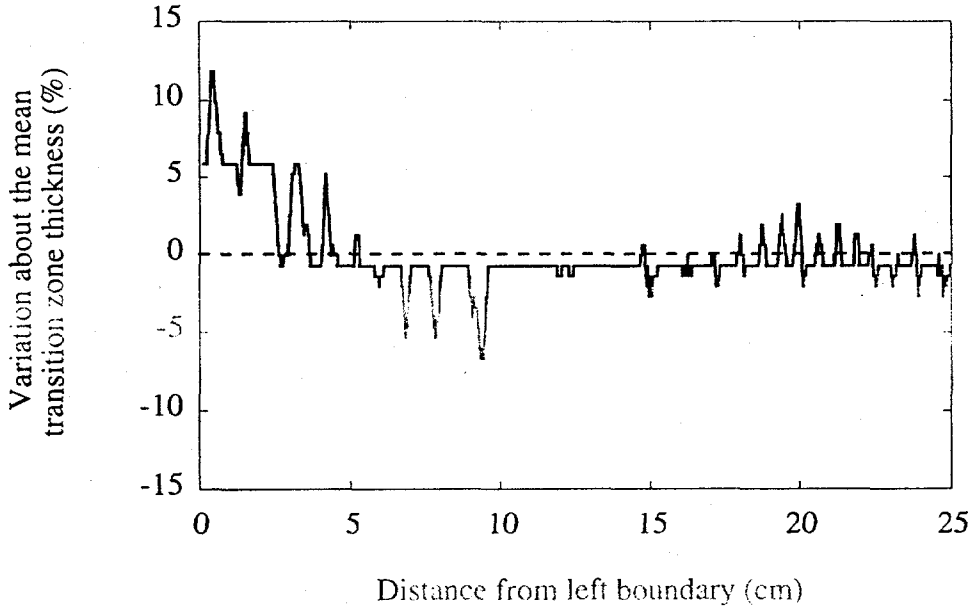
15
10
5
0
-5
-10
-15
0
5
10
15
20
25
Variation about the mean transition zone thickness (%)
Distance from left boundary (cm)

F4

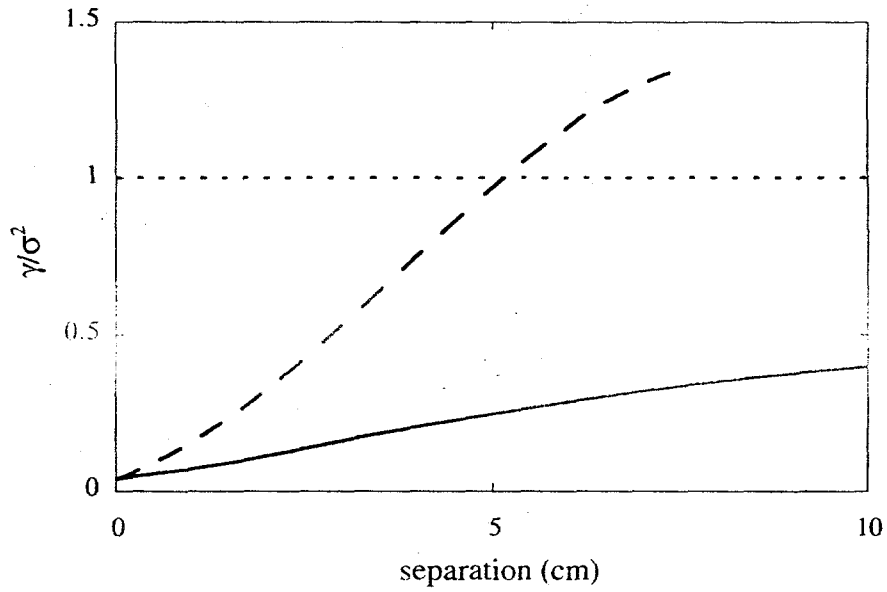

F5

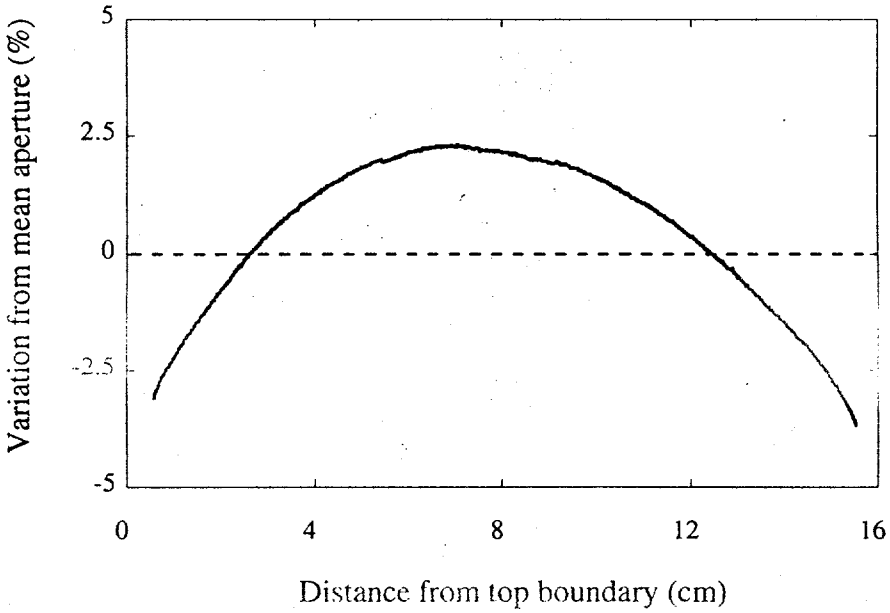
Variation from mean aperture (%)
5
2.5
0
-2.5
-5
0
4
8
12
16
Distance from top boundary (cm)

F6

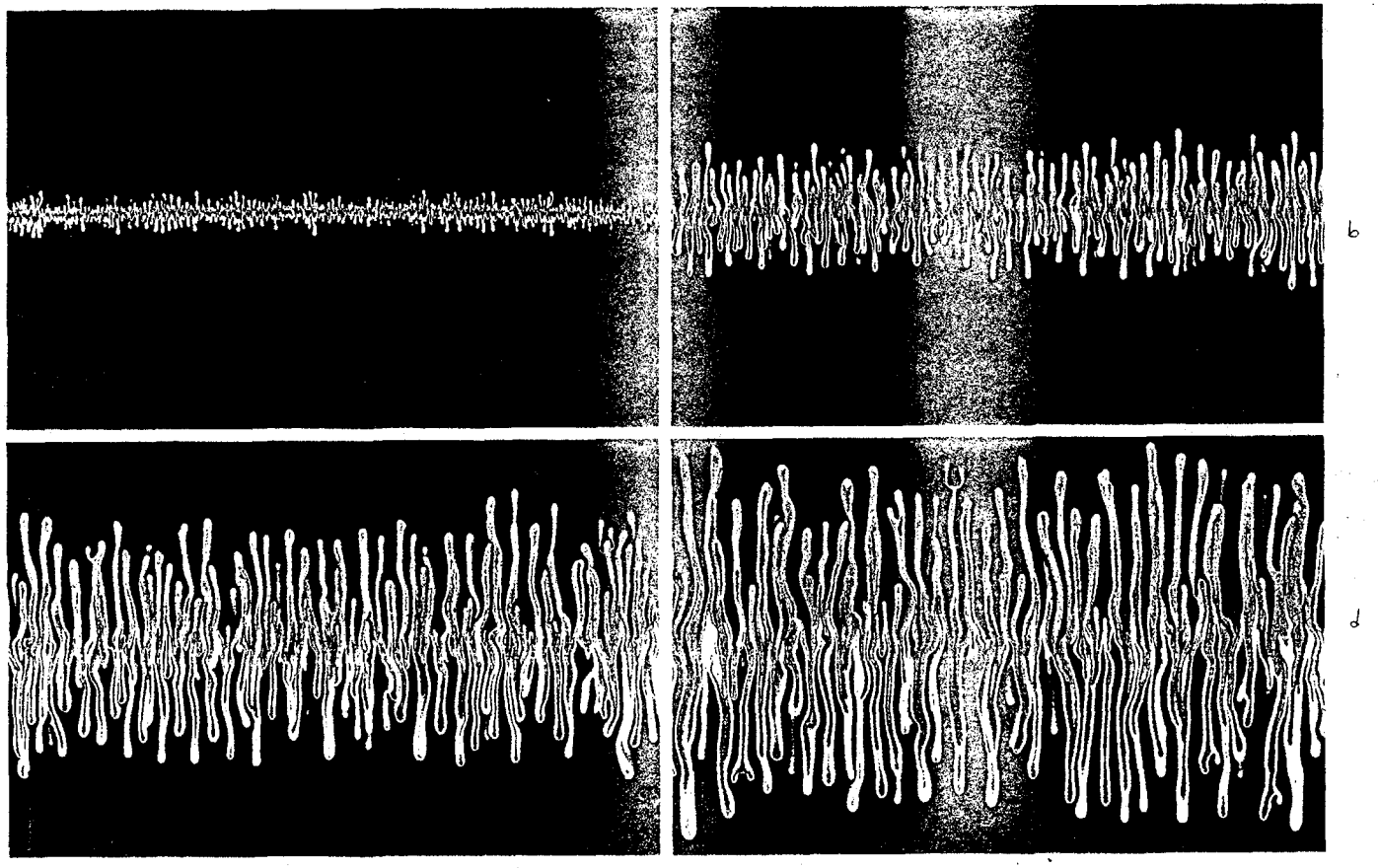

F 7

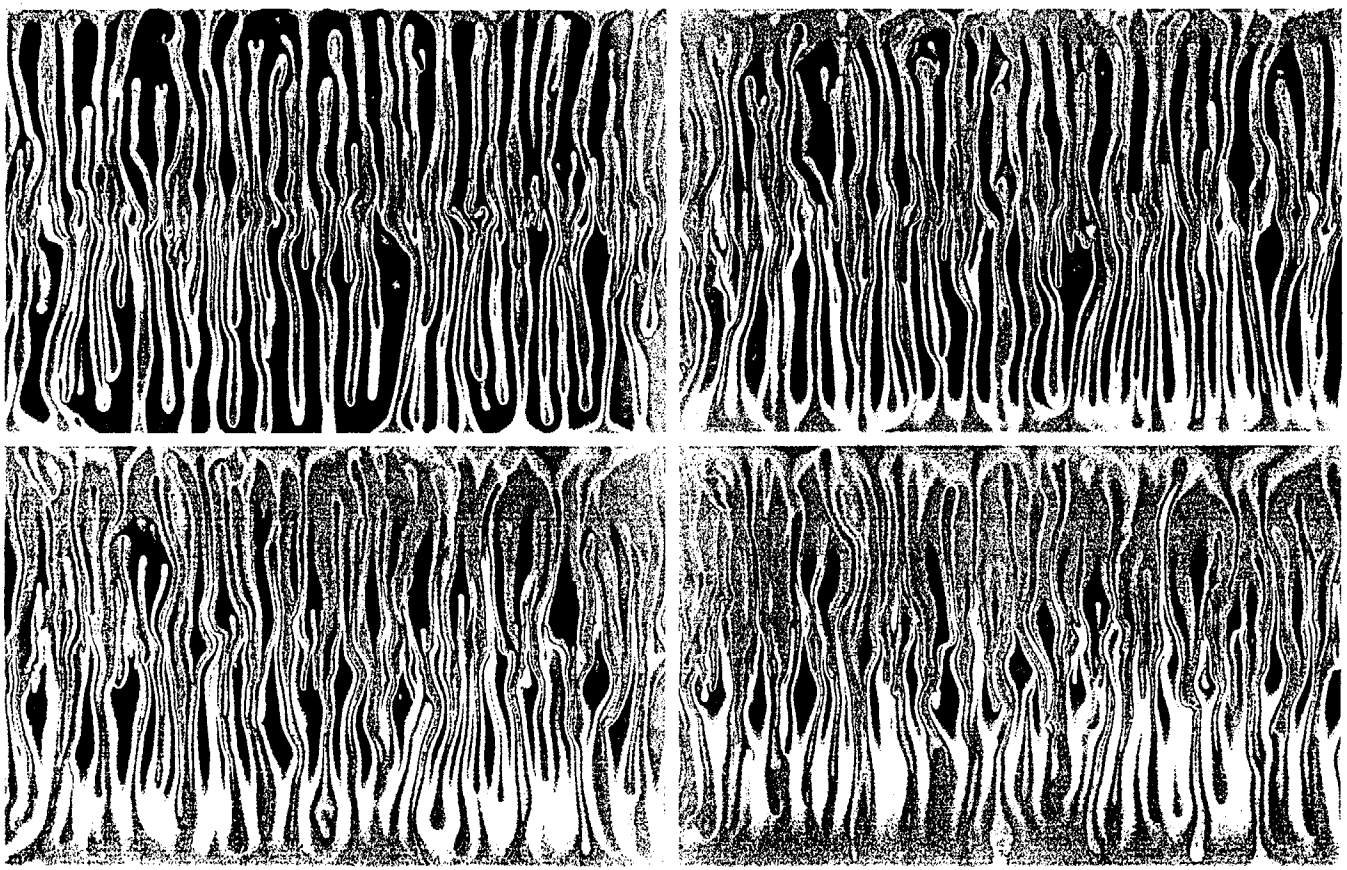

F7

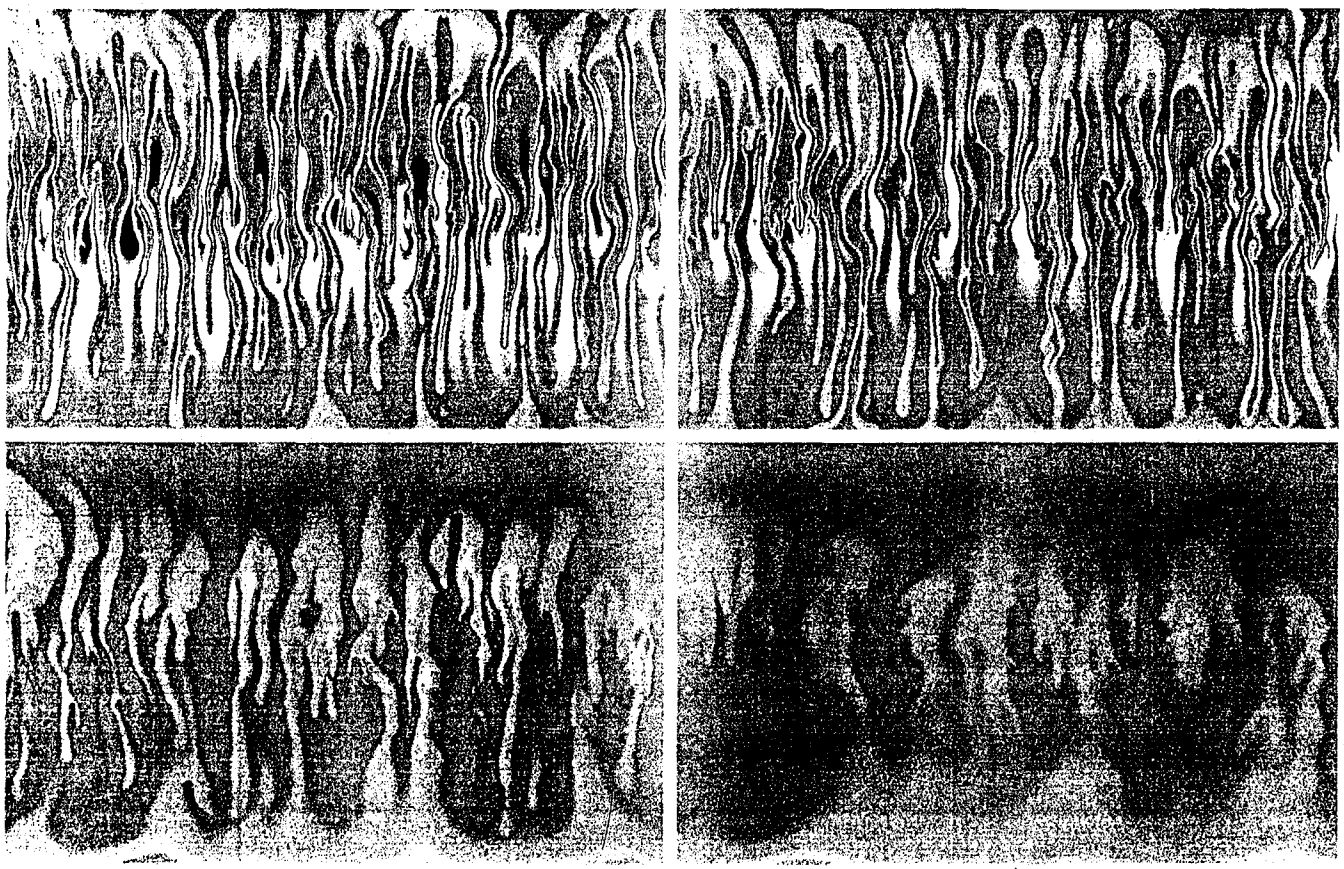
0
C/C0
1

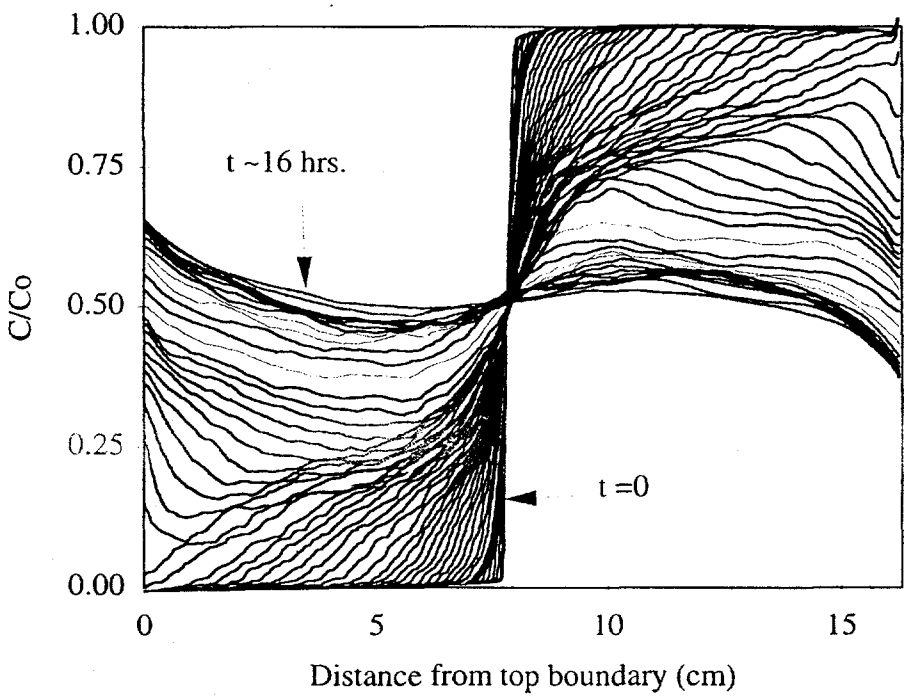
1.00
0.75
0.50
0.25
0.00
C/Co
t ~16 hrs.
t =0
0
5
10
15
Distance from top boundary (cm)

F 8

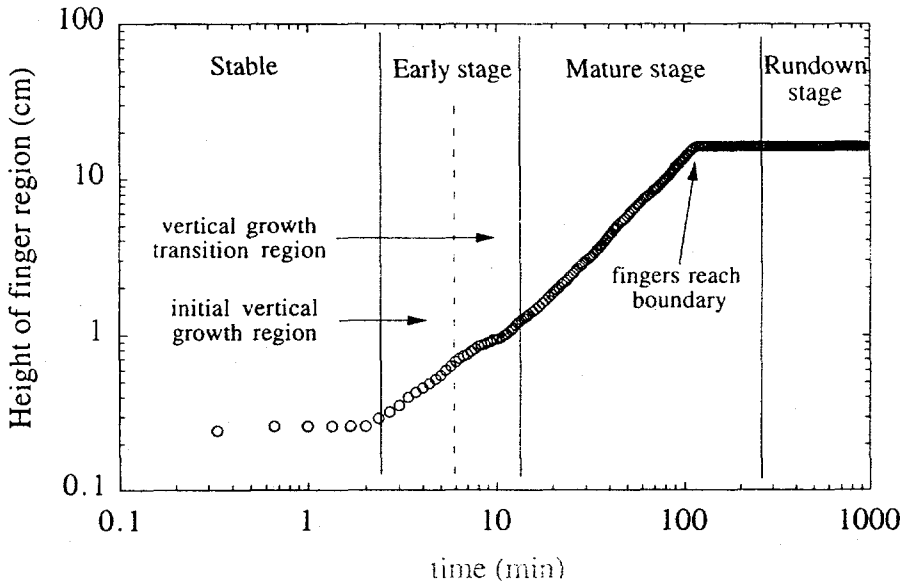
100
10
1
0.1
Height of finger region (cm)
Stable
Early stage
Mature stage
Rundown stage
vertical growth transition region
initial vertical growth region
fingers reach boundary
0.1
1
10
100
1000
time (min)

F 9

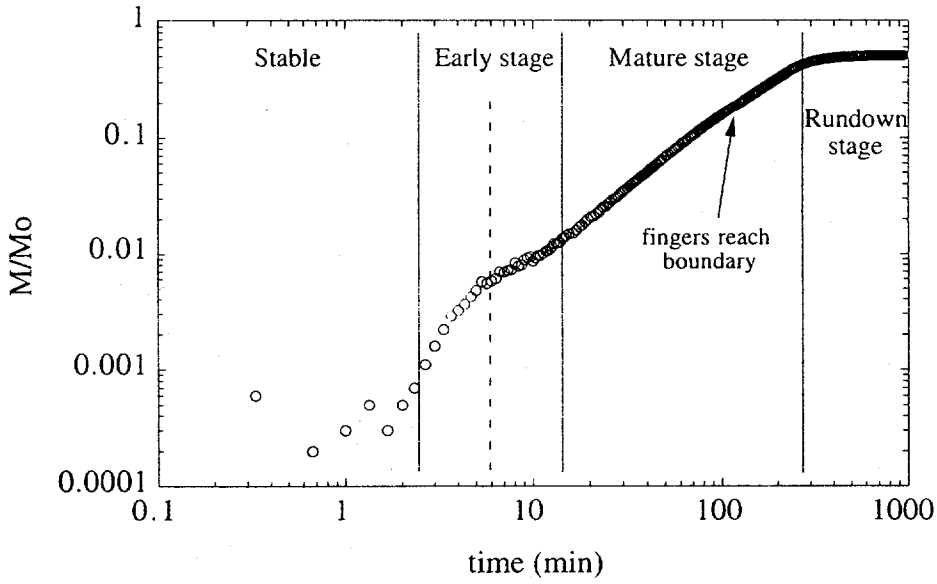
Stable
Early stage
Mature stage
Rundown stage
fingers reach boundary
M/Mo
1
0.1
0.01
0.001
0.0001
0.1
1
10
100
1000
time (min)

F10

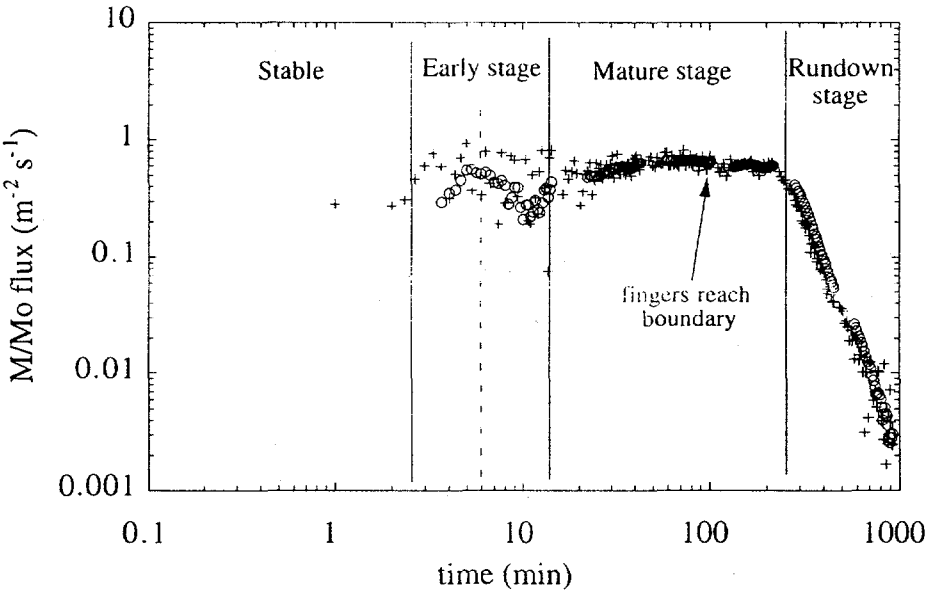
10
1
0.1
0.01
0.001
M/Mo flux (m-2 s-1)
Stable
Early stage
Mature stage
Rundown stage
fingers reach boundary
0.1
1
10
100
1000
time (min)

F 11

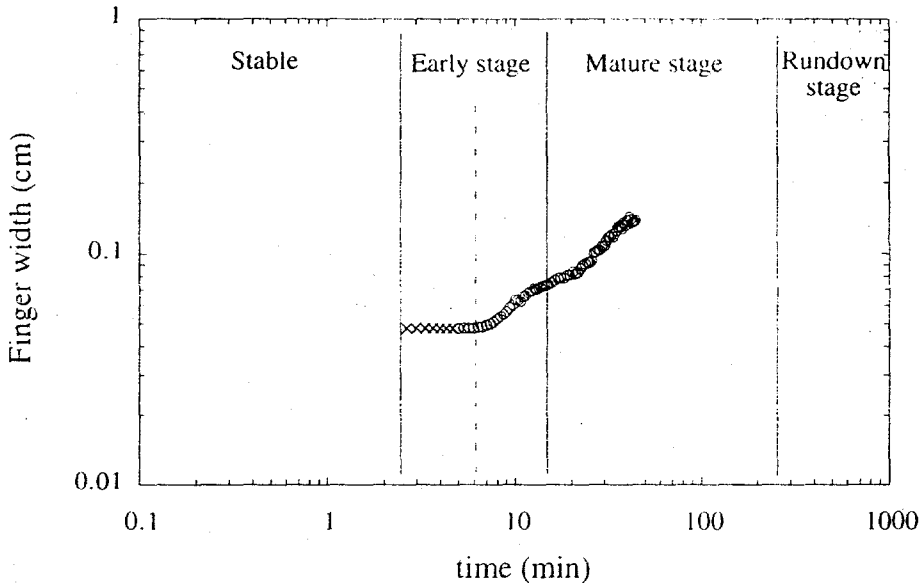
Stable
Early stage
Mature stage
Rundown stage
Finger width (cm)
1
0.1
0.01
0.1
1
10
100
1000
time (min)

F12